Bioconjugate Chemistry

ARTICLE

pubs.acs.org/bc

Self-Assembly Properties and Dynamics of Synthetic Proteo−Nucleic Building Blocks in Solution and on Surfaces

Aude Laisne,[†] Maxime Ewald,[‡] Toshio Ando,[§] Eric Lesniewska,[‡] and Denis Pompon*[,†]

[†]Centre de Génétique Moléculaire, CNRS, UPR3404, Avenue de la Terrasse, F91190 Gif-sur-Yvette, France

[‡]Institut Carnot Bourgogne, UMR CNRS 5209, University of Bourgogne, F21078 Dijon, France

[§]Department of Physics, Kanazawa University, Kakuma-machi, Kanazawa 920-1192, Japan

Supporting Information

ABSTRACT: Synthetic proteo−nucleic structures (PDNAs) encompassing a single-stranded DNA sequence covalently attached to a redox protein domain able to interact with surface or matrix were designed and characterized. They constitute versatile building blocks alternative to regular DNA for creating scaffolds with optical, electrical, or catalytic properties. PDNAs self-assemble in the presence of complementary oligonucleotides, to form a network of protein domains linked by double-stranded DNA segments. Electrophoretic and hydrodynamic behaviors of PDNAs and corresponding DNA were compared under electrophoresis and gel filtration conditions. Hybridization rates between small and large assemblies were characterized by rapid-mixing experiments. Results showed that the protein part significantly contributes to hydrodynamic behaviors of structures but marginally affects the conformation and hybridization properties of the nucleic domain. PDNA metal-mediated complexes with nitriloacetate-modified phospholipids can diffuse and interact at the surface of vesicles or supported membranes. Surface plasmon resonance analysis of membrane−PDNA interactions indicated that two protein units are required to allow stable surface association and that surface occupancy constrains assembly sizes. High-speed atomic force microscopy illustrated rapid lateral diffusion of assemblies on mica, revealing transient association between noncomplementary PDNA extremities and frequent trapping by surface defects. Regularly organized protein domains were visualized using a larger DNA framework.

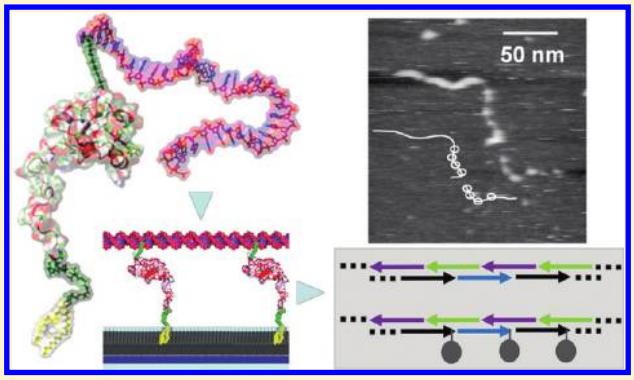

INTRODUCTION

The use of a synthetic DNA scaffold to build mono- or multidimensional nano-objects with fully predictable shapes rapidly developed as an important field of synthetic biology.[1−7] However, the limited range of functionalities that can be assembled using only nucleic acid tiles raised the question of the position specific incorporation of protein block in such scaffolds.[8] One way involved the DNA binding domain or the recognition of modified bases (for example biotin) by specific protein domains (avidin, antibodies, etc.).[8−11] Reciprocally, alternate approaches profit from the recognition of specific protein domains by aptamer structures embedded into the DNA scaffold.[12] However, these two methods suffer strong limitations because they require fusion of a large protein recognition domain to functional parts of interest or restrict the approach to structures for which suitable aptamers can be created. Protein−DNA recognition based on chemically mediated approaches (such as NTA−metal complexes) can also be considered, but either gives rise to reversible association or lacks specificity.[13,14]

PDNAs (protein−DNA structure), which are artificial structures that consist of a protein domain covalently linked to a single-stranded DNA (ssDNA) part through synthetic structures, constitute an attractive alternative.[15,16] The protein part of PDNA can be chosen to carry various types of functions such as surface interaction, binding, enzymatic, optical, or electrical properties, potentially creating nanostructures that can be used as biosensors[17,18] or active molecular devices. PDNA tiles can self-assemble in solution or be attached to a matrix in the presence of complementary ssDNA.[19] However, little is known about the stability and physicochemical and structural features of such objects or the ways they interact together compared to regular DNA tiles. This is particularly critical for defining methods adapted for specifically incorporating these building blocks into DNA scaffolds like origami[6] or other DNA-based supramolecular assemblies.[20]

This paper extends synthesis approaches for such PDNA building blocks and analyzes their physicochemical and assembly properties in comparison to their corresponding pure nucleotidic parts, at both global and single-molecule levels.

Received: May 2, 2011
Revised: July 8, 2011
Published: August 19, 2011

EXPERIMENTAL PROCEDURES

Synthesis of the PDNA Building Block. Oligonucleotides (Eurogentec) presented in section 1 of the Supporting Information were purified by ion-pairing reverse phase chromatography as previously described.[21] PDNAs were prepared by hemisynthesis from engineered human cytochrome b_5 (b_5) as described in sections 2 and 3 of the Supporting Information and previous work.[16,17,19] Briefly, a 3′- or internally amino linker-modified oligonucleotide was covalently attached through a disulfide bond to a modified b_5 containing a unique Cys residue and a His_4 C-terminal tag. During the synthesis, the amino linker of the ssDNA was coupled to a second linker terminated by a thiopyridine-protected thiol using NHS chemistry. A disulfide bond was finally formed by reacting the activated linker end with the unique Cys residue of the protein. The resulting products were purified to homogeneity by a combination of ion exchange and affinity chromatography, taking advantage of the protein His tag.

PDNA Thermal Stability. Experiments were performed in 20 mM Na/K phosphate buffer (pH 7.4) using PDNA or b_5 concentrations in the 10 μM range. Thermal denaturation was monitored on a Lambda 2 (Perkin-Elmer) spectrophotometer using increasing temperature steps of 4 °C. Spectra were recorded between 260 and 600 nm immediately after each temperature stabilization at a rate of 120 nm/min. Denaturation curves for native, engineered b_5, and PDNA were calculated from the changes in the 413 nm absorbance.

Phospholipid Vesicle Preparation. 1,2-Dimyristoyl-*rac*-glycero-3-phosphocholine (DMPC) was purchased from Sigma-Aldrich and 1,2-dioleoyl-*sn*-glycero-3-{[*N*-(5-amino-1-carboxypentyl)iminodiacetic acid]succinyl} (nickel salted) (DOGS-NTA) from Avanti Polar Lipids. A chloroform solution containing 1 mg of a DMPC/nickel DOGS-NTA mixture (90:10 molar ratio) was evaporated into a glass vial under a nitrogen flow, and the residue was dried under vacuum for 2 h. Phospholipids were hydrated overnight at 4 °C with 1.4 mL of 1× PBS buffer (Sigma-Aldrich), and the mixture was sonicated until a clear solution containing a total phospholipid concentration of 1 mM was obtained. The vesicles were extruded 19 times through polycarbonate membranes with 100 nm pores (Liposofast, Avestin).

Synthesis of Defined PDNA Assemblies. A detailed description is given in section 8 of the Supporting Information. Briefly, hybridizations of DNA and PDNA tiles were performed at 24 °C in 1× PBS buffer using a slight molar excess of DNA compared to PDNA. The constructs were purified from excess DNA either by association of IMAC and Sephadex G25/G50 chromatography or by HPLC size exclusion chromatography. The first method involved binding to an IMAC column (0.5 cm × 1.5 cm) and elution with a buffer supplemented with 30 mM histidine. EDTA (final concentration of 10 mM) was added to the eluate prior it being loaded onto a Sephadex G25 gel filtration column (0.5 cm × 1.5 cm) equilibrated with 1× PBS buffer. Alternatively, purification was performed by size exclusion chromatography (BioSuite 250, 4 μm UHR SEC, 4.6 mm × 300 mm, Waters) at a rate of 0.3 mL/min with 0.25 M NaCl and 0.15 M $NaKPO_4$ buffer (pH 6.8). DNA Ladders N3233 (Biolabs) were used for calibration.

Analysis of DNA and PDNA Hybridization Kinetics by Rapid-Mixing Experiments. Hybridization of simple DNA and PDNA tiles and preformed dimers was analyzed in rapid-mixing experiments by monitoring the hypochromic effect associated with the formation of double-stranded structures. Kinetic constants were calculated by fitting of the traces as described previously.[21]

Gel Filtration and Electrophoresis Methods. HPLC gel filtration analysis was performed on a Waters BioSuite 250 column (4 μm UHR SEC, 4.6 mm × 300 mm) at a rate of 0.3 mL/min with 0.25 M NaCl and 0.15 M $NaKPO_4$ buffer (pH 6.8). Sodium dodecyl sulfate−polyacrylamide gel electrophoresis (SDS−PAGE) analysis was performed using 4 to 12% NuPAGE Novex Bis-Tris polyacrylamide gels run at 24 °C and 120 V. Protein parts of PDNA were revealed by fast Coomassie blue staining and calibrated using the Mark12 Unstained standard from Invitrogen. Agarose gel analysis was performed using 3.5% NuSieve GTG Agarose from Tebu-bio in 1× TBE run at 50 V and 4 °C. DNA Ladders N3233 (Biolabs) were used for calibration. Agarose gel electrophoresis patterns were deconvoluted using an optimized expansion factor of 1.5 and band quantified as described previously for the analysis of regular DNA polymers.[21]

Surface Plasmon Resonance (SPR) Methods. SPR experiments were performed on a SPRi-Lab$^+$ array system (Genoptics) using 1× PBS as running buffer at a flow rate of 230 μL/min and 24 °C. Gold layer-covered prisms were cleaned by gentle sonication in a hot acid Pyranha solution (equal volume of 30% hydrogen peroxide and pure sulfuric acid), abundantly rinsed with Milli-Q water, and stored in pure HPLC grade acetonitrile until they were used. Experiments were performed following phospholipid vesicle fusion either on bare gold (lipid bilayer) or on a self-assembly monolayer of alkyl chains (lipid hemilayer). For that, the Pyranha-cleaned prism was immersed in a freshly prepared 1 mM solution of 1-octadecanethiol in ethanol (Sigma Aldrich) for 18 h and then rinsed with ethanol and water. Freshly extruded phospholipid vesicles (1 mM into 1× PBS buffer) were fused onto the treated substrate by circulation in the SPR cell at a flow rate of 50 μL/min for 30 min at 24 °C. An excess of adsorbed vesicles was removed by washing for 10 min with pure water (hypo-osmotic choc) followed by equilibration with 1× PBS buffer.

High-Speed Atomic Force Microscopy (HS-AFM). A laboratory-built high-speed atomic force microscope described previously was used to visualize the structure.[22−24] All observations were performed in oscillating contact mode in liquid. Small cantilevers designed for HS-AFM with a spring constant of 0.1−0.2 N/m, a resonant frequency of 0.8−1.2 MHz, and a quality factor of ∼2 in buffer solution were used.[25] The cantilever tips were grown by electron beam deposition (SEM Jeol 6500) and further sharpened by oxygen plasma etching (Plasma cleaner Harrick). The cantilever's free oscillation peak-to-peak amplitude (A_0) was set to 4−5 nm, while the feedback set point during imaging was set to ∼0.9 A_0. The samples were diluted (2−10-fold) in an observation buffer (OB) containing 10 mM $MgCl_2$. A drop (∼2 μL) was deposited on freshly cleaved green muscovite mica, and the mica was incubated at room temperature for 5 min. Subsequently, the mica surface was immersed in a liquid chamber filled with 60−100 μL of OB and subjected to HS-AFM. Diluted samples were used within a day (storage at 4 °C).

RESULTS

Three types of PDNAs including an engineered cytochrome b_5 redox domain and differing by the sequence of their nucleotidic parts and by the grafting position on the sequence of the

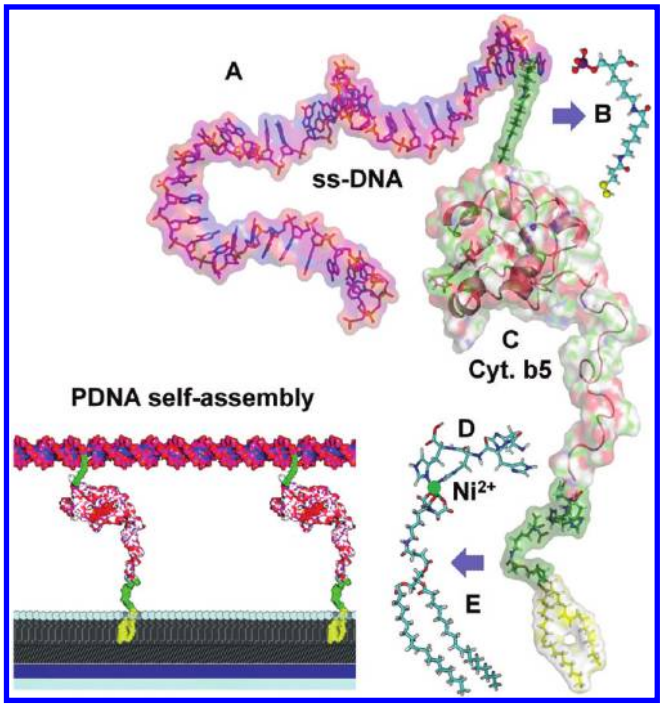

Figure 1. Structures of the PDNA building block, including a b_5 core. The structure is composed of a 39-base ssDNA part (A) attached either by its 3′-end (as illustrated) or by an internal amino C6 thymidine (not shown) to a synthetic linker (B) coupled to cytochrome b_5 (C) by the thiolate extremity of a cysteine at position 24. The His_4 C-terminal end (D) of the protein interacts with the nickel ion of an 18:1 DOGS-NTA-modified lipid (E). The structure at the bottom left shows PDNA blocks inserted into a dsDNA structure. The structure is floating on a supported membrane composed of a phospholipid monolayer covering a self-assembled octadecanethiol monolayer on gold.

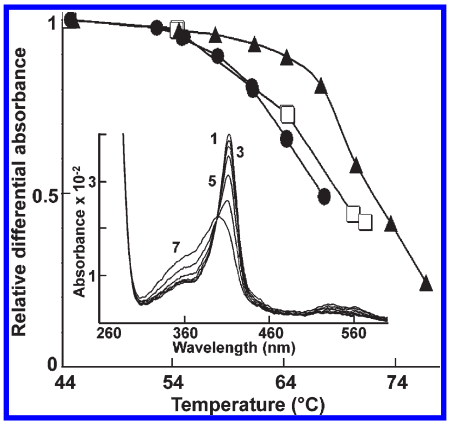

Figure 2. Thermal stabilities of b_5 folding in wild-type, Cys-modified, and corresponding PDNA structures. Protein denaturation was monitored by observation of the spectral changes of the bound heme cofactor at 413 nm. Denaturation curves were compared for native (▲), Cys-modified b_5 (□), and PDNA (●) forms. Typical spectral changes following incubation of a PDNA at temperatures increasing from 44 to 68 °C in steps of 4 °C are illustrated in inset curves 1 (44 °C) to 7 (68 °C).

protein domain (Figure 1, right) were prepared by hemisynthesis and purified to homogeneity (sections 2 and 3 of the Supporting Information). In these structures, the protein C-terminal His tag

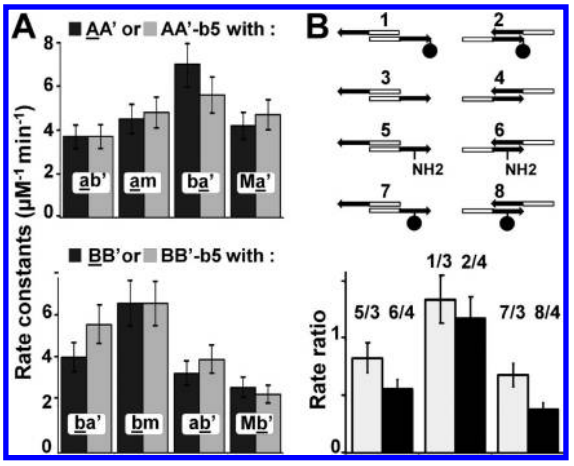

Figure 3. Comparative rate constants for DNA and PDNA hybridizations. (A) Hybridizing oligonucleotides are indicated inside bars (matching segments underlined). Dark and light gray boxes refer to hybridization of DNA and corresponding PDNA to half-cDNA, respectively. Second-order rate constants were deduced from measurements of the hypochromic effect in rapid-mixing experiments. (B) Ratios among hybridization rates for normal, base-modified, and protein-coupled oligonucleotides. These ratios are defined by a scheme in which the circle stands for the protein domain and the NH2 label for the internal base modification. White and black bars correspond to hybridizations involving the distal and proximal segments of oligonucleotides, respectively.

plays an important role in permitting the formation of a metal chelate linkage between the PDNAs and Ni-NTA groups attached to either a polymer matrix, modified phospholipids, or functionalized surfaces. Lateral diffusion of anchored PDNAs remains possible either by stepwise release and rebinding of the metal chelate or, in the case of vesicles or a supported membrane, through lipid diffusion. Hybridization of the PDNA single-stranded part to complementary nucleic acid generates a more rigid double-stranded DNA (dsDNA) structure (Figure 1, left) that, depending on sequences, could self-organize into a wide range of nucleo−proteic networks. Such structures can alternatively be made by substituting the cytochrome b_5 domain with any other protein of interest provided that a single grafting point can be engineered at the surface.

Stability and Hybridization Properties of the PDNA Building Block in Solution. The termal stability of the PDNA protein domain under conditions required for hybridization reactions is critical for the maintenance of the functional integrity and particularly redox properties. This was analyzed in solution by monitoring the temperature-dependent disruption of the cytochrome b_5 absorption spectra, which tightly depend on the iron coordination by two histidine residues of the protein. Results indicated that the reversible denaturation of the protein part of the PDNA is observed only above 55 ± 2 °C, a value identical to that found for the DNA-free engineered protein and slightly lower (2−3 °C) than that for the native protein (Figure 2). Oxidoreduction properties of the cytochrome b_5 domain in PDNA structures were found to be conserved. An identical transition in the absorption spectra, which is characteristic of the redox change of the histidine-coordinated iron porphyrin, was observed upon electron transfer in the native protein and on PDNA structures. Thus, the presence of the ssDNA part has no significant effect on the stability and redox properties of the protein domain. The thermal stability of the protein is sufficiently

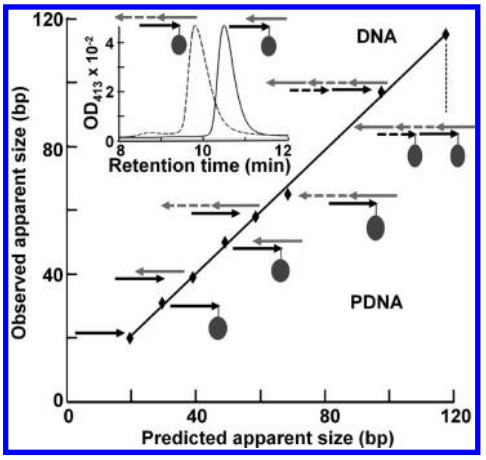

Figure 4. Size exclusion chromatography characterization of short PDNA assemblies. Structures depicted were analyzed on a HPLC gel filtration column (detection at 413 and 254 nm) and apparent molecular masses calculated using dsDNA as molecular mass standards. Apparent molecular masses (expressed in base pairs) were predicted using the formula molecular mass (base pairs) = $10P + 0.5S + D$, where P, S, and D stand for the number of protein unit(s) (●) and ss- and dsDNA bases (arrows), respectively. The inset shows experimental peak shapes for illustrated constructs.

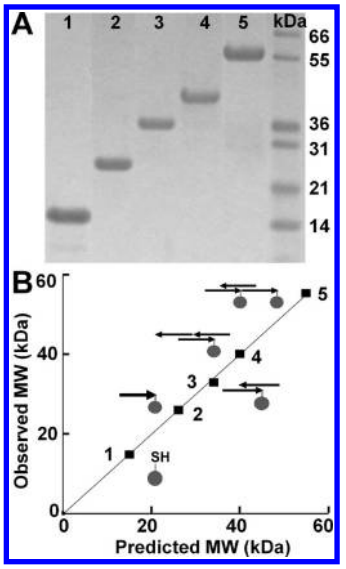

Figure 5. SDS−PAGE analysis of short PDNA assemblies. (A) Experimental gel, in which the numbering of lanes corresponds to the structure depicted in the bottom panel. (B) Relation between the observed molecular mass (calculated on the basis of a protein standard) and those predicted using the formula molecular mass (kilodaltons) = $15P + 0.282S + 0.359D$, where P, S, and D stand for the number of protein unit(s) (●) and ss- and dsDNA bases (arrows), respectively. Structures 2−4 are derived from AA′-b5 PDNAs, and structure 5 combines AA′-b5 and BB′-b5 PDNAs.

high to allow hybridization to proceed under classical conditions (55 °C) for oligonucleotides.

Reciprocally, the effect of the protein domain on the hybridization properties of the DNA domain was investigated for structures in which covalent grafting was performed either internally or at the 3′-end of the oligonucleotidic part. Monitoring of hypochromic effects was used to analyze the relative rates of hybridization of the different PDNAs with complementary ssDNA sequences. To discriminate between hydrodynamic and protein-related microenvironment effects, hybridization properties were analyzed on both the proximal and the distal sides (3′- and 5′-halves, respectively) of the nucleic part of PDNAs. In addition, the potential influence of the nature (ds- vs ssDNA) of the region flanking the hybridization site was investigated.

During hybridization of PDNAs, protein absorption at 260 nm represents less than 10% of the nucleic acid absorbance and does not contribute to spectral changes. Second-order hybridization rate constants ranging from 1.9 to 7 μM^{-1} min^{-1} were observed (Figure 3), while the lengths of the hybridizing segments were almost identical (19−20 bases) in all experiments. Comparison of hybridization rates for DNA and 3′-end-grafted PDNA with an identical sequence indicated that protein-dependent modulation of rates is limited with regard to the effects related to the sequence of hybridizing segments (Figure 3A). Moreover, analysis of the relative rates of hybridization events occurring in the distal and proximal parts of PDNA confirmed a hardly significant influence of the protein domain when grafted at the 3′-end of the nucleic part (labels 1/3 and 2/4 in Figure 3B). In contrast, when the grafting was performed internally in the nucleic part, a more significant effect on rates was observed, which resulted both from the presence of a modified base in the hybridizing segment (labels 5/3 and 6/4 in Figure 3B) and the attachment of the protein domain (labels 7/3 and 8/4). In both cases, distal grafting has a limited influence compared to proximal grafting, suggesting that the effect relates more directly to protein−DNA interaction rather than to changes in the global hydrodynamic properties in solution.

Electrophoretic and Chromatographic Properties of PDNA Assemblies of Increasing Sizes. To further investigate the relations between hydrodynamic behaviors and structures, different types of PDNA assemblies were built. The relative contributions of protein and nucleic domains were analyzed using a series of constructs built from hybridization-driven assembly of two PDNA tiles (or corresponding DNA controls), namely, AA′-b5 and BB′-b5 (section 1 of the Supporting Information). The AA′ PDNA building block was designed to hybridize with the 5′-half of ab′ and the 3′-half of ba′ cDNA, matching their a and a′ parts, respectively. Similarly, the BB′ PDNA block can hybridize to ba′ and ab′ DNA tiles by matching their b and b′ parts, respectively. The complementary tiles were assembled by single-step or sequential (purification of intermediates) hybridizations at low (25−45 °C) temperatures followed by final purification to homogeneity by combinations of Ni-NTA affinity and gel filtration chromatography to resolve PDNA assemblies from excess DNA. Corresponding structures and HPLC gel filtration profiles are illustrated in Figure 4. Individual constructs migrate during gel filtration as Gaussian-shaped bands, allowing easy determination of their relative mobility under the high-salt buffer conditions required to prevent interaction with the silica matrix of columns. Interestingly, DNA and protein structural elements contributed in a perfect additive way to the apparent size calculated on the basis of dsDNA standards. The individual contributions of the ssDNA (0.5 bp/base), dsDNA (1 bp/bp), and protein (equivalent to 10 bp/unit) parts appeared to be independent of the assemblies considered. Consequently, the plot of the apparent sizes versus calculated values for eight different constructs is linear. The 10 bp/unit equivalent contribution of the protein part corresponds to an apparent molecular mass of 6.6 kDa, a value significantly

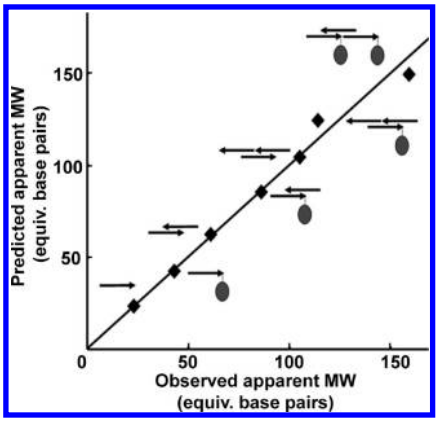

Figure 6. Agarose gel analysis of the apparent molecular mass of PDNA and DNA assemblies. Structures depicted on the figure were resolved by 3.5% agarose gel electrophoresis in 1× TBE. Calibration was performed with dsDNA standards. Molecular masses were predicted using the formula molecular mass (base pairs) = $25P + 0.6S + D$ for DNA−DNA constructs and the formula molecular mass (base pairs) = $25P + 1.55S + D$ for PDNA−DNA constructs, where P, S, and D stand for the number of protein units, ssDNA bases, and dsDNA base pairs, respectively.

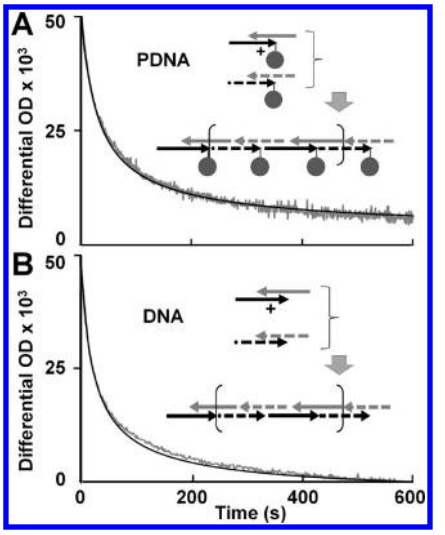

Figure 7. Rapid-mixing analysis of the formation of tile concatemers. (A) Experimental (gray line) and simulated (black line) kinetic courses for the copolymerization of the depicted preformed PDNA−DNA hybrids. (B) Same data for the hybridization of corresponding DNA−DNA hybrids. Simulations were performed using rate constants from Figure 3A and parameters from section 6 of the Supporting Information.

smaller than its actual size of 13 kDa, which would correspond to smaller hydrodynamic radii for proteins compared to those of dsDNA standards with identical masses. However, this is not consistent with predicted hydrodynamic radii[26,27] that are similar (1.9−2 nm) for a dsDNA of 13 kDa (20 bp) and for the b_5 core (13 kDa). The difference can be related to the flux-dependent hydrodynamic stretching that is expected to occur and affect differentially globular and linear structures in the tightly packed HPLC gel filtration column.

To gain additional insight, the electrophoretic mobility of the different constructs was evaluated under SDS−PAGE conditions (Figure 5). Analysis illustrated that coupling of the DNA parts to the protein induces a strong shift in mobility. The apparent molecular mass increases from ∼15 kDa for the b_5 core alone to 27 kDa for the corresponding single-stranded PDNA, the difference of 12 kDa being consistent with the molecular mass (∼13 kDa) of the DNA part. This result contrasts with gel filtration data and could appear surprising as the protein and DNA parts exhibit very different permanent charges. However, protein in SDS−PAGE is expected to be denatured into an extended and rather rigid form and negatively charged by the interacting SDS.[28] SDS-denatured protein and dsDNA have thus some common conformational features that de facto result in identical electrophoretic mobilities for similar masses. In contrast, the contribution to the apparent molecular mass of the ssDNA part was consistently found to be ∼50% larger than that of the dsDNA part for equivalent masses with a lower persistence length of ssDNA compared to that of dsDNA.

The conformation of PDNA-based structures in solution was analyzed using nondenaturing agarose gel electrophoresis (Figure 6). An additive contribution to the apparent size (expressed as base pair equivalents) of PDNA assembly components was observed as described previously with ssDNA, dsDNA, and protein parts contributing to ∼0.6, 1, and 25 bp equivalents, respectively (section 4 of the Supporting Information). The 16.5 kDa protein contribution is close to the 15 kDa value determined by SDS−PAGE, while calibration was performed using dsDNA standards. This feature is the reciprocal of the situation found for DNA calibrated on a protein standard using SDS−PAGE. It suggests that the folded b_5 core has electrophoretic mobility similar to that of dsDNA with the same mass in agarose gels. Likewise, the relative apparent masses of ss- and dsDNA are similar in the two electrophoretic systems. However, analysis of the electrophoretic mobilities of DNA and PDNA polymers evidenced that the contribution of ssDNA to the apparent molecular mass differs in PDNA (1.55−1.78 bp/base) and DNA (0.60−0.69 bp/base) assemblies (section 4 of the Supporting Information). The effect is identical with one or several protein units per construct and suggests that the presence of protein affects the contribution to mobility of linked ssDNA but not of dsDNA (section 4 of the Supporting Information). This phenomenon was not observed during gel filtration where the protein is folded but an electrical field is absent or during SDS−PAGE where the protein domain is unfolded.

Hybridization Properties of Large PDNA-Based Structures. While hybridization properties of defined small PDNA and corresponding DNA structures appeared to be very similar, we questioned the behavior of larger assemblies in which protein content could significantly impact geometry and steric hindrance causing topological restriction to base pairing. The model used was the formation of block copolymers involving regular repeats of two types of PDNAs. When AA′ and BB′ PDNA were mixed with half-complementary tiles (ab′ and ba′), a polymer featuring AA′-BB′ PDNA repeats can be formed. The reaction was first monitored using the hypochromic effect resulting from the hybridization of single-stranded sticky ends. Panels A and B of Figure 7 compare the reaction courses for PDNA−DNA and DNA−DNA polymerization, respectively. Individual rate constants described in Figure 3 were used to simulate the reaction courses using the same modeling approaches[21] for PDNA and DNA assemblies. This model assumes that hybridization rates of large polymer fragments decrease with a power of −0.57 of species length for DNA.[21,29] For PDNA, an equivalent length was

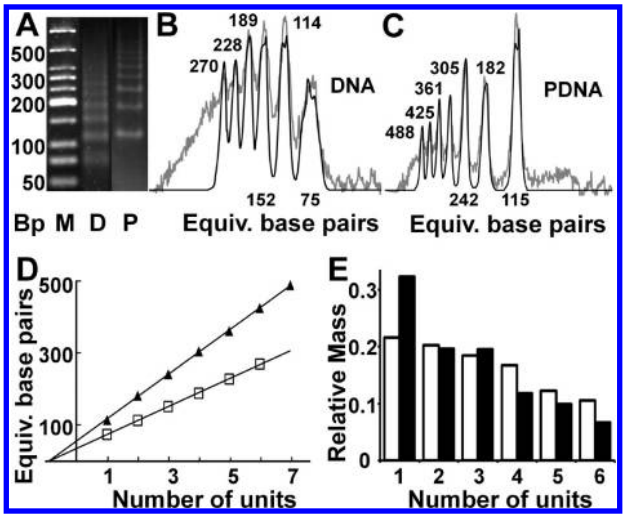

Figure 8. Size distribution of DNA and PDNA copolymers. (A) Agarose gel electrophoresis of DNA and PDNA polymer distribution after polymerization for 10 min of the four reactant tiles at ~1 μM each and quenching with ~1.5 μM terminator tiles (section 6 of the Supporting Information). (B and C) Scans of the experimental gel profiles (gray lines) and their deconvolution (black lines) for DNA and PDNA, respectively. (D) Plot of the dsDNA equivalent size of PDNA (▲) and DNA (□) polymers vs the number of units. Slopes correspond to 67 and 40.5 bp/unit for PDNA and DNA, respectively. (E) Quantification as equivalent masses of bands from panels B (white bars) and C (black bars) as a function of polymer size. The error in band quantification depends on methods but does not exceed a relative error of 10−15%.

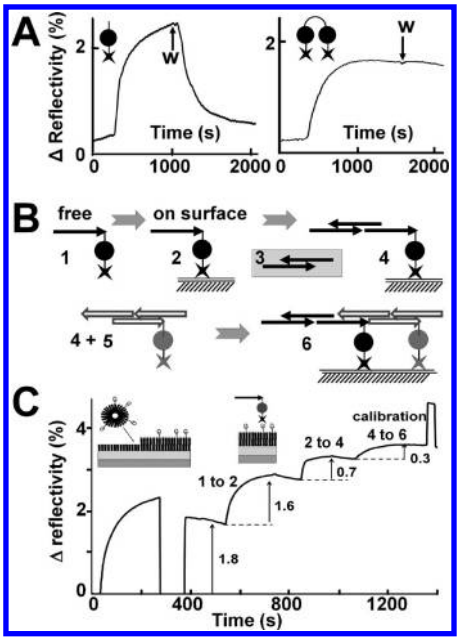

Figure 9. SPR analysis of the interaction of PDNA assemblies and of their b_5 component with phospholipids. (A) Binding kinetics of the b_5 component of PDNAs in the monomeric state (left) or following protein dimerization through a disulfide bond (right). The W label denotes the start of the washing phase. (B) Step by step self-assembly of PDNAs on a membrane surface. Free PDNA (1), supported membrane-bound PDNA (2), free DNA−tile dimer (3), coupling product of steps 2 and 3 (4), free hybrid (5) between one PDNA and two DNA tiles, and coupling product of steps 4 and 5 (6). (C) SPR sensorgram corresponding to panel B. The numbers correspond to steps depicted in panel B. The differential reflectivity for each step is indicated by the arrows.

calculated as the sum of the real size of the nucleic part and of a contribution of the protein equivalent to 10 dsDNA bases per protein unit. This value was set to be identical to the protein contribution evidenced in gel filtration experiments. The figure illustrates that experimental courses were well-simulated with this same model for DNA- and PDNA-based experiments. This indicates that, for large linear assemblies, no significant additional factor, which could differentiate PDNA from DNA, needs to be taken into account to describe the global behavior.

For further comparison, the size distribution of polymer species was analyzed by gel electrophoresis and profiles were deconvoluted as previously described[21] to calculate the electrophoretic mobility and for quantification (Figure 8A−C). However, in this case, terminator tiles (namely, am, Ma′, bm, and Mb′) able to cap the free ssDNA parts (A, A′, B, and B′, respectively) of polymer extremities have to be added to quench the polymerization and allow gel electrophoresis analysis. The quenching process was incorporated into the simulation model (sections 5 and 6 of the Supporting Information).[21] For DNA and PDNA polymers, the apparent size was found to be proportional to the number of repeats with an additional contribution of single-stranded quencher ends (Figure 8D). As expected, the size step between bands appeared to be significantly larger for PDNA (~65 bp equivalent) than for DNA (40 bp equivalent) because of the contribution of protein domains to PDNA. However, relative distributions of polymer concentration obtained in DNA−DNA and PDNA−DNA experiments were found to be similar (Figure 8E) and consistent with simulations. At this point, we can conclude that DNA and PDNA recognition in solution is fully driven by the nucleic acid part with almost undetectable interference of the protein domain, except for hydrodynamic effects associated with size differences.

Self-Assembly of PDNAs on Vesicles and Supported Membranes. The protein domain of PDNA carries a C-terminal His_4 tag that can form a complex with nickel, cobalt, or copper divalent ions, mediating association through a surface and thus constraining self-assembly mechanisms. While the affinity of short His tag sequences for the nickel-nitriloacetate linker is sufficient for tight binding on affinity columns, the lifetime of such a complex is fairly short, generally a few seconds.[14,30−32] Binding of the PDNA protein part to the phospholipid bilayer supplemented with DOGS-Ni was evaluated using 100 nm calibrated liposomes. The protein and phospholipid saturation curves are illustrated in section 7 of the Supporting Information. Half-saturation for the monomeric b_5 domain used in PDNA construction was found to be ~5 μM, and the binding capacity was clearly proportional to the total phospholipid concentration, leading to an average binding surface of ~50 nm^2 for a single b_5 unit.

Assembly of PDNA on a membrane was further investigated using a DOGS-NTA-Ni-doped hemimembrane supported on gold, which allows monitoring of assembly by surface plasmon resonance (SPR). Figure 9A illustrates that the binding of the protein part of PDNA to the supported membrane is efficient but rapidly reversible with an affinity in the micromolar range, confirming the previous observation with vesicles. However, when the protein parts form a dimeric structure, a stable association is observed with a dissociation rate hardly measurable (hour

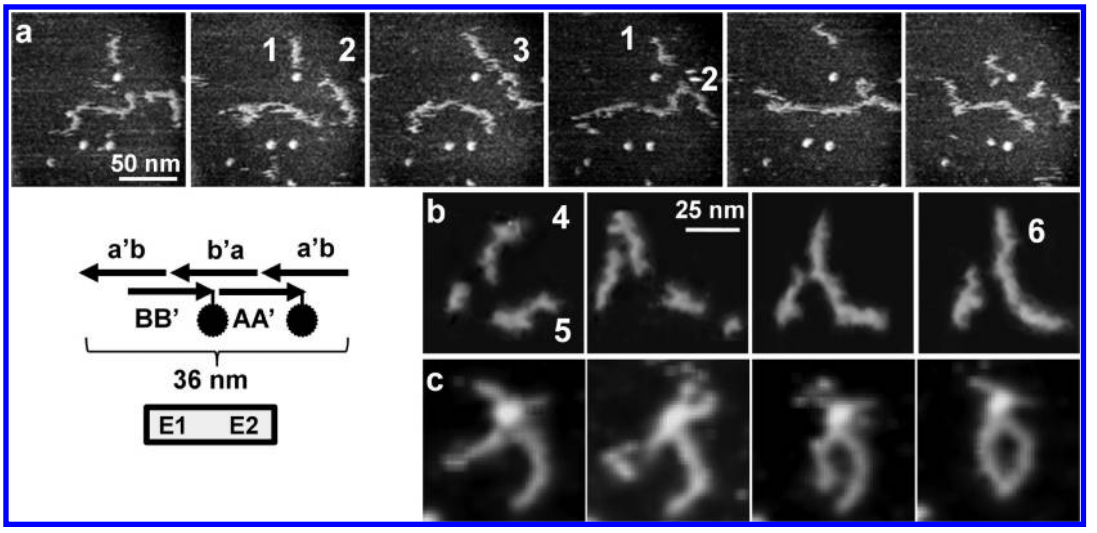

Figure 10. High-speed AFM analysis of the dynamics of PDNA structures. (a and b) Dynamic AFM imaging (10 frames/s) evidencing the formation of transient concatemers (species 1 and 2 giving 3 and 4 and 5 giving 6) of the construct described in the scheme. (c) Dynamics of two constructs anchored onto a nanoparticle. Images from lane a were untreated, while nonrelevant background noise was removed for the sake of readability in lanes b and c.

range). This is due to a rebinding process in the diffusion limit layer immediately surrounding the surface when at least two linkages exist between the object and the surface. Such a situation typically occurs when two PDNA tiles become linked through hybridization with a cDNA tile. This principle is used in the experiment described in Figure 9B and is illustrated by the SPR sensorgram in Figure 9C. Formation of a supported membrane hemilayer is evidenced by the fusion of DOGS-Ni-supplemented phospholipid vesicles onto alkane thiol-modified gold. Binding of PDNA to the Ni-NTA lipid head (steps 1 and 2) appeared to be efficient, and the trace clearly illustrates that the bound PDNA can be easily hybridized (steps 2−4) with the complementary extremity of a DNA−DNA half-hybrid that acts as a linker between two PDNAs (steps 4−6) finally stabilizing the whole construct on the surface. However, the addition of mass following hybridization appeared to be significantly below the expected stoichiometry, and the defect increased with a larger number of assembly steps. This could be explained by the fact that binding of additional PDNA tiles to the surface is sterically impaired by tiles already associated on the surface. Reducing the effect would need careful control of surface saturation during assembly initiation. However, this would suppose working under conditions far from surface saturation, which would in turn dramatically reduce the magnitude of the SPR signal, making multiple-step assemblies difficult to monitor.

AFM Analysis of the Dynamics and Interactions of Short PDNA Assemblies. A construct encompassing two PDNA tiles (scheme in Figure 10) was prepared and adsorbed onto freshly cleaved mica in the presence of magnesium. High-speed AFM imaging evidenced lateral mobility with large changes in position (tens of a nanometer) and shapes of objects within the 100 ms time lapse between two scans (Figure 10a). An overlay of consecutive images separated by a 100 ms time lapse on a 300 nm × 300 nm scale illustrates the presence in the population of lower-mobility segments, while other regions of the molecules were rapidly laterally diffusing (image sequence available in section 9 of the Supporting Information). Surface defects, such as nanoparticles a few nanometers in diameter, can very efficiently trap diffusing PDNA structures, anchoring them onto a specific point of the surface when the remaining parts are still stochastically moving around leading to tweezerslike structures (Figure 10a, lane 3). Interestingly, two or more constructs can frequently interact together, resulting in the apparent fusion of objects to give unstable longer species (Figure 10a, lane 2). The events appeared to be mostly conservative with respect to length

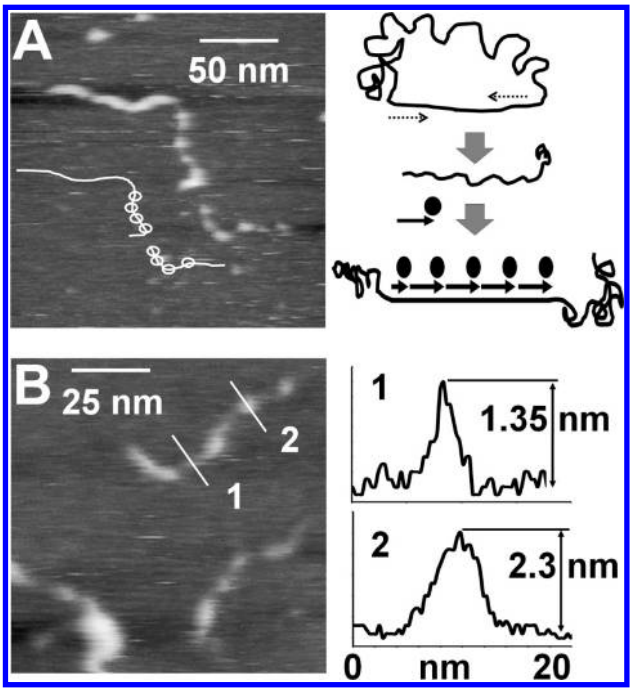

Figure 11. Structures of immobilized PDNA assemblies. (A) High-speed AFM imaging (raw data) of two assemblies and a schematic description of the image. (B) Three other objects are illustrated at a higher resolution (raw data), and section profiles of the DNA (1) and protein (2) parts are given. Constructs encompassing five PDNA units hybridized to a large single-stranded DNA were prepared as outlined in the right part of the scheme (see section 8 of the Supporting Information for details).

(daughter species has a length close to the sum of the parents), a feature expected for classical base pairing. However, the construct exhibits single-stranded extremities that are not complementary and cannot give rise to a stable duplex. Consistently, the species appeared to be monodisperse in gel electrophoresis. However, formation during gel filtration of shoulder peaks with molecular masses greater than that of the main species suggested weak interactions of construct extremities, consistently with predicted ΔG values of −7.8 (b/b), −7.5 (a′/a′), and −3.6 kcal/mol (b/a′) for the formation of intermolecular hydrogen bonds in a salty solution (section 10 of the Supporting Information). Such energies are sufficient to create short life (few seconds) but easily observable concatemers under dynamic AFM conditions. Statistical analysis of the length distribution of the concatemer (one to eight repeats) was performed on 106 objects, and the resulting profiles were found to be consistent with a model in which single-stranded extremities of the species interact together on the surface with ΔG values of −1.8 and −0.8 kcal/mol, respectively (section 11 of the Supporting Information). The observation was found to be dentical upon imaging of DNA and PDNA of identical nucleotidic structures. As a control, concatenation events were never observed with a dsDNA (513 bp) that does not include single-stranded extremities.

Structural Analysis of Large PDNA Structures. It could appear surprising that the protein domains were hardly visible under previously used experimental conditions. However, the linker attaching DNA and protein domains in PDNA is sufficiently flexible to allow fairly different dynamics for the two components. Under previously used conditions, the scanning rate probably remained too slow compared to the dynamics of the protein domain to capture the 2 nm globular structural details. To limit the overall dynamics, larger objects were designed, including a 513-base single-stranded DNA scaffold on the middle of which up to five PDNA tiles can be hybridized (Figure 11A). As previously reported,[33] ssDNA segments generate tightly folded regions strongly interacting with the substrate. Under such conditions, a string of protein domains (thickness of 2.3 nm) regularly placed (10−15 nm) along the DNA filament (thickness of 1.35 nm) can clearly be imaged by high-speed AFM. Control involving dsDNA with same sequence illustrates a filament with a homogeneous thickness of ∼1.3 nm (not shown). This illustrates that PDNA building blocks can be easily used to decorate a DNA scaffold.

DISCUSSION

Covalent coupling of protein and DNA domains into a single building block is a versatile alternative to noncovalent complexes for building proteo−nucleic structures.[34−37] Different PDNAs encompassing a cytochrome b_5 protein domain linked to a ssDNA were designed, synthesized, and purified to homogeneity. The C-terminal His tag on the protein part offers a way to create more specific and localized interactions with substrates than DNA alone that nonspecifically interacts with ion-doped material like Ni^{2+}-treated mica.[33] The requirement to build PDNAs is the availability of a unique grafting position in the protein sequence. Use of a surface cysteine residue is a method of choice, but alternate solutions include the use of a rare or non-natural amino acid like a selenocysteine or an *N*-acetylphenylalanine,[38] which can be selectively grafted using adapted chemistry. A generic approach could also involve grafting of the surface cysteine opposite the CDR3 binding region onto small (14 kDa) VHH single-chain antibodies. Such antibodies could be used in turn to form a noncovalent high-affinity complex with any protein of interest.[39]

This work specifically aimed to compare the physicochemical and self-assembly properties of DNA and PDNA in different environments. Defining and controlling parameters implied in self-assembly mechanisms of such hybrid synthetic structures will permit us not only to use them as modular building blocks for multifunctional nanostructures but also to improve our understanding of properties of natural nucleo−proteic complexes. A contribution of the protein domain to the hydrodynamic properties of PDNAs was clearly evidenced by gel filtration and electrophoresis in SDS−PAGE and nondenaturing agarose gels. In all cases, the protein contribution appeared to be additive with respect to the one of the nucleic acid parts provided to use an equivalent DNA length that differs depending on the analysis method considered. During gel filtration, the 13 kDa protein domain migrates like a solvated dsDNA of 6.6 kDa. This contrasts with an equivalent mass of 16−17 kDa observed in nondenaturing agarose gel electrophoresis calibrated using dsDNA. This last value is consistent with a mass of 15 kDa for the protein domain in SDS−PAGE following calibration with proteins. This is in agreement with a common extended conformation of the reference molecules (DNA and protein) used for calibration in an agarose gel and during SDS−PAGE, respectively. During HPLC gel filtration, hydrodynamic constraints resulting from flow are expected to favor a rather extended conformation of the DNA used for size calibration. In contrast, the protein domain remains globular, which tends to decrease its relative apparent size. Reciprocally, during agarose gel electrophoresis, the much lower charge of the protein domain compared to that of DNA decreases the relative protein mobility, thus compensating for the more compact structure of the protein domain. The strictly additive contributions of double-stranded nucleic and protein domains to hydrodynamic behaviors for a variety of PDNA assemblies suggested that conformational interactions between the two components are likely weak under all tested conditions and do not affect their individual shapes.

In contrast to pure nucleic structures that are generally assembled under conditions close to the melting temperature to avoid formation of dead-end parasitic hybrids,[6,20] proteo−nucleic structures must be preferentially assembled in a kinetically controlled manner,[40−42] far below the melting temperature to prevent thermal denaturation of protein domains. Hybridization rates are thus critical parameters of PDNAs that were analyzed by monitoring hypochromic effects associated with hybridization in rapid-mixing experiments. While the length of hybridizing segments is homogeneous for all considered tiles, observed hybridization rates significantly differ over a 4-fold range. This dispersion does not simply correlate with obvious sequence features and for the same hybridizing segment depends on the nature of flanking regions. The reason is likely related to the formation of possible secondary structures of ssDNA parts, some of them having predicted stability sufficiently large (8−14 kcal/mol) to significantly interfere. In contrast, comparison of the hybridization rates of DNA and corresponding PDNA does not evidence a significant effect of the protein domain when grafted on the oligonucleotide 3′-end. However, a moderate decrease in hybridization rates was observed for internal grafting proximal to the hybridizing segment. In this case, base modification by the linker and protein presence exhibited cumulative effects. When hybridization between larger polymers was considered, no additional effect

was observed compared to the situation with short building blocks, suggesting the absence of long-range interaction between PDNAs when formation of linear polymer was considered.

Altogether, our results indicate that DNA and PDNA tiles are mostly equivalent at the level of their hybridization properties and that PDNA can easily substitute for DNA in most DNA-based supramolecular assemblies, provided that the folding can sterically accommodate the protein parts. A potential limitation remains the thermal stability of the protein domain under the fairly high-temperature conditions required to prevent formation of a dead-end product by spurious hybridization.[6,43] However, analysis of the thermal stability of our constructs evidenced that linkage to the nucleic acid part has no significant detrimental influence on protein stability leading, in our case, to constructs stable up to 55 °C, a value that is compatible with current hybridization procedures. Thus, any reasonably stable protein can be substituted for our cytochrome b_5 domain, including recognition protein-like single-chain antibodies of the VHH family. In the case of very unstable protein domains, an alternative assembly procedure under kinetic control remains possible using, for example, DNA hairpin or loop motifs as programmable units.[41,44] A combination of kinetic and thermodynamic control can also be used to direct self-assembly processes by engineering intra- and interparticle DNA hybridization.[5,45]

PDNAs potentially offer many advantages when self-assemblies on surfaces are targeted. The protein domain can be used, for example, for the recognition of surface chemical or physical features using material specific affinity domains.[46] This also applies to redox active proteins (like cytochrome b_5), for which electron transfer properties at surface interfaces can be modulated by the conformation of the DNA scaffold, thus constituting biosensors. Analysis by rapid-scan AFM clearly evidenced lateral diffusion properties of PDNA assemblies on surfaces. SPR experiments demonstrated that such structures can be sequentially built by stepwise extension from a matrix-bound primer[19] or by self-organization of tiles attached to membranes (this work). However, the progressive yield decrease during constructions resulted either from surface saturation or, as shown by HS-AFM, from the presence of surface defects able to anchor laterally diffusing PDNA molecules. A possible turnaround to build defect-free surfaces would be the use of phospholipid vesicles as assembly frame. This work illustrates that the fairly limited stability of the attachment of PDNA to NTA-modified phospholipids is a limitation, which could be somewhat overcome when several protein modules are bound to the same vesicles. Alternatively, multiple-head NTA constructs can be used to increase affinity.[13,14,30−32] However, the fairly rigid structure of large PDNA−DNA supramolecular assemblies was found to conflict with the strong curvature of small (50−100 nm) vesicles and more importantly can reciprocally induce an unwanted phase transition of the support phospholipid structures, leading to uncontrolled organization.

Formation of transient end-to-end concatemers was evidenced by HS-AFM upon lateral diffusion of PDNA assemblies on the surface. Similar behavior was observed when DNA was substituted with PDNA under the same experimental conditions. The phenomenon was clearly related to the presence of ssDNA extensions on constructs that can form short stretches of paired bases (four to six bases) and was not observed with fully dsDNA. Interaction energies deduced from modeling of the concatemer distribution appeared to be ∼4-fold smaller than calculated values in solution, which is consistent with the much lower salt concentration used under AFM imaging conditions. Formation of these transient structures while they are reversible competes with true hybrid formation during assemblies slowing the process on surfaces. The phenomena could be enhanced by the presence of surface defects that efficiently trap diffusing PDNA assemblies and by the observed topological cluttering on the surface (AFM and SPR experiments). These three effects combine in reducing the self-assembly efficiency of surface-bound objects.

While high-speed AFM opens a new dimension for the analysis at the single-molecule level of nucleic acid assemblies, difficulties could arise from the relative values of scan rate and object dynamics. Our data evidence that the small b_5 domain (13 kDa) was not visible when attached to highly dynamic structures, whereas it was clearly imaged when bound to much larger DNA exhibiting a lower mobility. Thus, it seems that some compromise has to be found between resolution and dynamic analyses, particularly when very small objects are involved. While dynamic AFM observation of a fairly small protein (calmodulin, 17 kDa) bound to a streptavidin crystal was recently reported,[47] our results go further than previous reports[48] by visualizing for the first time a small protein domain (13 kDa) linked to isolated DNA molecules in solution.

■ ASSOCIATED CONTENT

Supporting Information. DNA tile sequences and matches (section 1), schematic for the synthesis of protein−DNA (PDNA) structures (section 2), synthesis of PDNA structures (section 3), contribution of building blocks to the apparent size in gel filtration and electrophoresis (section 4), experimental and simulated profiles for PDNA copolymers (section 5), parameter sets for simulations (section 6), cytochrome b_5 and phospholipid concentration dependence for the formation of protein−lipid complexes (section 7), purification of the DNA and PDNA assemblies described here (section 8), high-speed AFM image sequences (section 9), thermodynamic parameters (section 10), and statistical analysis of the formation of concatemers (section 11). This material is available free of charge via the Internet at http://pubs.acs.org.

■ AUTHOR INFORMATION

Corresponding Author

*Telephone: +33 567048806. Fax: +33 561559400. E-mail: denis.pompon@insa-toulouse.fr. Present address: LISBP/INSA, UMR INSA/CNRS 5504, 135 Avenue de Rangueil, 31077 Toulouse cedex 4, France.

Funding Sources

We acknowledge the financial support of this work by Grants ANR-05-NANO-021-04, ANR-08-NANO-010-01, and ANR-08-PCV08_343399 from the Programme Nanosciences et Nanotechnologies (PNANO) and Programme interdisciplinaire en physique et chimie du vivant (PCV) actions of the National Research Agency (ANR), France.

■ ACKNOWLEDGMENT

We thank Dr. Takayuki Uchihashi (Physics Laboratory, Kanazawa University), Drs. Ignacio Casuso and Simon Sheuring (Institute Curie, Paris, France), Dr. Pierre-Emmanuel Milhiet

(CBS, Montpellier, France) for technical support, and Dr. Gilles Truan for proofreading the manuscript.

REFERENCES

(1) Brucale, M., Zuccheri, G., and Samori, B. (2006) Mastering the complexity of DNA nanostructures. *Trends Biotechnol. 24*, 235–243.

(2) He, Y., Tian, Y., Chen, Y., Deng, Z., Ribbe, A. E., and Mao, C. (2005) Sequence Symmetry as a Tool for Designing DNA Nanostructures. *Angew. Chem., Int. Ed. 44*, 6694–6696.

(3) Ke, Y., Liu, Y., Zhang, J., and Yan, H. (2006) A study of DNA tube formation mechanisms using 4-, 8-, and 12-helix DNA nanostructures. *J. Am. Chem. Soc. 128*, 4414–4421.

(4) Liu, Y., Ke, Y., and Yan, H. (2005) Self-assembly of symmetric finite-size DNA nanoarrays. *J. Am. Chem. Soc. 127*, 17140–17141.

(5) Rotello, V. M. (2009) DNA nanotechnology: Hot and sticky or cold and aloof. *Nat. Mater. 8*, 539–540.

(6) Rothemund, P. W. (2006) Folding DNA to create nanoscale shapes and patterns. *Nature 440*, 297–302.

(7) Seeman, N. C. (1998) DNA nanotechnology: Novel DNA constructions. *Annu. Rev. Biophys. Biomol. Struct. 27*, 225–248.

(8) Teller, C., and Willner, I. (2010) Organizing protein-DNA hybrids as nanostructures with programmed functionalities. *Trends Biotechnol. 28*, 619–628.

(9) Yan, H., Park, S. H., Finkelstein, G., Reif, J. H., and LaBean, T. H. (2003) DNA-templated self-assembly of protein arrays and highly conductive nanowires. *Science 301*, 1882–1884.

(10) Park, S. H., Pistol, C., Ahn, S. J., Reif, J. H., Lebeck, A. R., Dwyer, C., and LaBean, T. H. (2005) Finite-Size, Fully Addressable DNA Tile Lattices Formed by Hierarchical Assembly Procedures. *Angew. Chem., Int. Ed. 45*, 735–739.

(11) Beyer, S., Nickels, P., and Simmel, F. C. (2005) Periodic DNA nanotemplates synthesized by rolling circle amplification. *Nano Lett. 5*, 719–722.

(12) Liu, Y., Lin, C., Li, H., and Yan, H. (2005) Aptamer-directed self-assembly of protein arrays on a DNA nanostructure. *Angew. Chem., Int. Ed. 44*, 4333–4338.

(13) Conti, M., Falini, G., and Samori, B. (2000) How Strong Is the Coordination Bond between a Histidine Tag and Ni - Nitrilotriacetate? An Experiment of Mechanochemistry on Single Molecules. *Angew. Chem., Int. Ed. 39*, 215–218.

(14) Lata, S., Reichel, A., Brock, R., Tampe, R., and Piehler, J. (2005) High-affinity adaptors for switchable recognition of histidine-tagged proteins. *J. Am. Chem. Soc. 127*, 10205–10215.

(15) Boireau, W., Bombard, S., Sari, M. A., and Pompon, D. (2002) Bioengineering and characterization of DNA-protein assemblies floating on supported membranes. *Biotechnol. Bioeng. 77*, 225–231.

(16) Boireau, W., Duncan, A. C., and Pompon, D. (2005) Bioengineering and characterization of DNA-protein assemblies floating on supported membranes. *Methods Mol. Biol. 300*, 349–368.

(17) Boireau, W., Zeeh, J. C., Puig, P. E., and Pompon, D. (2005) Unique supramolecular assembly of a redox protein with nucleic acids onto hybrid bilayer: Towards a dynamic DNA chip. *Biosens. Bioelectron. 20*, 1631–1637.

(18) Berthier, A., Elie-Caille, C., Lesniewska, E., Delage-Mourroux, R., and Boireau, W. (2008) Nanobioengineering and Characterization of a Novel Estrogen Receptor Biosensor. *Sensors 8*, 4413–4428.

(19) Pompon, D., and Laisne, A. (2007) PDNA as building blocks for membrane-guided self-assemblies. *Biochem. Soc. Trans. 35*, 495–497.

(20) Rothemund, P. W., Papadakis, N., and Winfree, E. (2004) Algorithmic self-assembly of DNA Sierpinski triangles. *PLoS Biol. 2*, e424.

(21) Laisne, A., Lesniewska, E., and Pompon, D. (2011) Design and experimental validation of a generic model for combinatorial assembly of DNA tiles into 1D-structures. *Biochim. Biophys. Acta 1810*, 603–611.

(22) Ando, T., Kodera, N., Takai, E., Maruyama, D., Saito, K., and Toda, A. (2001) A high-speed atomic force microscope for studying biological macromolecules. *Proc. Natl. Acad. Sci. U.S.A. 98*, 12468–12472.

(23) Ando, T., Uchihashi, T., Kodera, N., Yamamoto, D., Miyagi, A., Taniguchi, M., and Yamashita, H. (2008) High-speed AFM and nano-visualization of biomolecular processes. *Pfluegers Arch. 456*, 211–225.

(24) Ando, T., Uchihashi, T., Kodera, N., Yamamoto, D., Taniguchi, M., Miyagi, A., and Yamashita, H. (2007) High-speed atomic force microscopy for observing dynamic biomolecular processes. *J. Mol. Recognit. 20*, 448–458.

(25) Kitazawa, M., Shiotani, K., and Toda, A. (2003) Batch Fabrication of Sharpened Silicon Nitride Tips. *Jpn. J. Appl. Phys. 42*, 4844–4847.

(26) Garcia De La Torre, J., Huertas, M. L., and Carrasco, B. (2000) Calculation of hydrodynamic properties of globular proteins from their atomic-level structure. *Biophys. J. 78*, 719–730.

(27) Robert, C. H. (1995) Estimating friction coefficients of mixed globular/chain molecules, such as protein/DNA complexes. *Biophys. J. 69*, 840–848.

(28) Reynolds, J. A., and Tanford, C. (1970) The gross conformation of protein-sodium dodecyl sulfate complexes. *J. Biol. Chem. 245*, 5161–5165.

(29) Sorlie, S. S., and Pecora, R. (1990) A dynamic light scattering study of four DNA restriction fragments. *Macromolecules 23*, 487–497.

(30) Huang, Z., Hwang, P., Watson, D. S., Cao, L., and Szoka, F. C., Jr. (2009) Tris-nitrilotriacetic acids of subnanomolar affinity toward hexahistidine tagged molecules. *Bioconjugate Chem. 20*, 1667–1672.

(31) Huang, Z., Park, J. I., Watson, D. S., Hwang, P., and Szoka, F. C., Jr. (2006) Facile synthesis of multivalent nitrilotriacetic acid (NTA) and NTA conjugates for analytical and drug delivery applications. *Bioconjugate Chem. 17*, 1592–1600.

(32) van Broekhoven, C. L., and Altin, J. G. (2005) The novel chelator lipid 3-(nitrilotriacetic acid)-ditetradecylamine (NTA(3)-DTDA) promotes stable binding of His-tagged proteins to liposomal membranes: Potent anti-tumor responses induced by simultaneously targeting antigen, cytokine and costimulatory signals to T cells. *Biochim. Biophys. Acta 1716*, 104–116.

(33) Maeda, Y., Matsumoto, T., and Kawai, T. (1999) Observation of single- and double-stranded DNA using non-contact atomic force microscopy. *Appl. Surf. Sci. 140*, 400–405.

(34) Endo, M., and Sugiyama, H. (2009) Chemical approaches to DNA nanotechnology. *ChemBioChem 10*, 2420–2443.

(35) Niemeyer, C. M. (2001) Semi-synthetic nucleic acid-protein conjugates: Applications in life sciences and nanobiotechnology. *J. Biotechnol. 82*, 47–66.

(36) Niemeyer, C. M. (2007) Functional devices from DNA and proteins. *Nano Today 2*, 42–52.

(37) Niemeyer, C. M. (2010) Semisynthetic DNA-protein conjugates for biosensing and nanofabrication. *Angew. Chem., Int. Ed. 49*, 1200–1216.

(38) Liu, C. C., and Schultz, P. G. (2010) Adding new chemistries to the genetic code. *Annu. Rev. Biochem. 79*, 413–444.

(39) Kastelic, D., Frkovic-Grazio, S., Baty, D., Truan, G., Komel, R., and Pompon, D. (2009) A single-step procedure of recombinant library construction for the selection of efficiently produced llama VH binders directed against cancer markers. *J. Immunol. Methods 350*, 54–62.

(40) Lubrich, D., Green, S. J., and Turberfield, A. J. (2009) Kinetically controlled self-assembly of DNA oligomers. *J. Am. Chem. Soc. 131*, 2422–2423.

(41) Shih, W. (2008) Biomolecular assembly: Dynamic DNA. *Nat. Mater. 7*, 98–100.

(42) Wieland, M., Benz, A., Haar, J., Halder, K., and Hartig, J. S. (2010) Small molecule-triggered assembly of DNA nanoarchitectures. *Chem. Commun. 46*, 1866–1868.

(43) Winfree, E., Liu, F., Wenzler, L. A., and Seeman, N. C. (1998) Design and self-assembly of two-dimensional DNA crystals. *Nature 394*, 539–544.

(44) Yin, P., Choi, H. M., Calvert, C. R., and Pierce, N. A. (2008) Programming biomolecular self-assembly pathways. *Nature 451*, 318–322.

(45) Leunissen, M. E., Dreyfus, R., Cheong, F. C., Grier, D. G., Sha, R., Seeman, N. C., and Chaikin, P. M. (2009) Switchable self-protected attractions in DNA-functionalized colloids. *Nat. Mater. 8*, 590–595.

(46) Seeman, N. C. (2002) Key experimental approaches in DNA nanotechnology. *Current Protocols in Nucleic Acid Chemistry*, Chapter 12, Unit 12, p 1, Wiley, New York.

(47) Yamamoto, D., Nagura, N., Omote, S., Taniguchi, M., and Ando, T. (2009) Streptavidin 2D crystal substrates for visualizing biomolecular processes by atomic force microscopy. *Biophys. J. 97*, 2358–2367.

(48) Lyubchenko, Y. L., and Shlyakhtenko, L. S. (2009) AFM for analysis of structure and dynamics of DNA and protein-DNA complexes. *Methods 47*, 206–213.